KeAi
CHINESE ROOTS
GLOBAL IMPACT

Available online at www.sciencedirect.com

ScienceDirect

Advances in Climate Change Research 13 (2022) 196–204

www.keaipublishing.com/en/journals/accr/

Improvements on the upper-ocean simulation from 2007 to 2018 in the Canada Basin

Long-Jiang MU[a], Xiao-Yu WANG[a,b,*]

[a] *Pilot National Laboratory for Marine Science and Technology (Qingdao), Qingdao 266237, China*
[b] *Frontier Science Center for Deep Ocean Multispheres and Earth System (FDOMES), Physical Oceanography Laboratory, Ocean University of China, Qingdao 266100, China*

Received 14 April 2021; revised 10 September 2021; accepted 17 December 2021
Available online 23 December 2021

Abstract

The Beaufort Gyre reserves most of the freshwater in the Arctic Ocean. Observation shows that the freshwater content over 2016–2018 far exceeds the level over the plateau period 2008–2012. Modeling the vertical temperature and salinity structure and their changes in the Beaufort Gyre is a way to understand the process related to such step changes. We configured a pan-Arctic sea ice-ocean model with a southern boundary at ~7°N in the Atlantic Ocean. The numerical simulation with sea surface salinity restoring, a latitude dependent horizontal diffusivity scaled by the squared buoyancy frequency, and a weak vertical diffusivity of 5×10^{-7} m^2 s^{-1} in the Arctic Ocean better reproduces the sea ice extent, the Pacific summer halocline water, and the freshwater variations as observed. The sea surface salinity restoring mitigates the surface desalination in the North Atlantic Ocean, therefore a weaker ocean stratification prevents the excessive warming in the intermediate Arctic Ocean. It is also found that the weak vertical background diffusivity is the major factor in our model to preserve the vertical ocean structure in the Canada Basin and also the step change of freshwater recently. In addition to resolving eddy activities in high resolution models, the success in our low resolution model suggests that tuning the vertical diffusivity serves as another approach to simulate the increasing freshwater content in the recent decade.

Keywords: Beaufort Gyre; Numerical simulation; Upper Arctic Ocean; Freshwater content

1. Introduction

The Arctic Ocean is undergoing dramatic changes over recent decades (e.g., Stroeve and Notz, 2015). A prominent phenomenon documented by abundant studies and widespread social media is the significant sea ice decline starting from the early 21st century. The sea ice retreat not only in extent but also in thickness (Tilling et al., 2015) drives more socioeconomic activities in the Arctic, as an example, the number of voyages through the Northeast Passage has increased from 75 in 2016 to 156 in 2019 in March, and from 345 to 447 in September according to the statistics from the Nord University. Scientific researchers observe twice atmospheric warming in the Arctic than in the mid-latitudes, which is known as Arctic amplification (e.g., Serreze and Barry, 2011), accompanying with abundant accumulation of liquid freshwater in the Arctic Ocean (e.g., Proshutinsky et al., 2009; Rabe et al., 2014).

The Canada Basin is the largest freshwater reservoir in the Arctic Ocean. Variations of freshwater content (FWC) are modulated by the Beaufort High (Proshutinsky et al., 2009). The prevailing high pressure system drives an anticyclonic circulation in the Beaufort Gyre with freshwater accumulation caused by strong Ekman pumping. Observations from the

* Corresponding author. Qingdao National Laboratory for Marine Science and Technology, Qingdao 266237, China.
E-mail address: xywang@ouc.edu.cn (WANG X.-Y.).
Peer review under responsibility of National Climate Center (China Meteorological Administration).

https://doi.org/10.1016/j.accre.2021.12.004

Beaufort Gyre Exploration Project maintained by the Woods Hole Oceanographic Institution show a strong freshwater increasing over the period 2003–2007 (https://www.whoi.edu/website/beaufortgyre/data). In the following five years from 2008 to 2012, the FWC changes rather minor, but a sudden drop occurred in 2013. Based on a model study, Wang et al. (2018a) suggested that strong cyclonic winds in 2012, which cause upward Ekman pumping to release the FWC remarkably thereafter, induces the 2013 recorded low in recent years. However, the freshwater starts its recharge very fast after 2013 and exceeds the 2003–2007 level in 2015.

The simulation of such strong interannual variability is a challenge in the state-of-the-art models. The simulated FWC variability tends to be weaker than the observed estimate. Hu et al. (2019) found that FWC is not maintained after 2008 in their ocean model with horizontal resolution of 12 km, while the model with higher resolution (~4.5 km) reproduces realistic FWC variability. They concluded that eddy activities in the Arctic in high resolution models contribute to the lateral flux which helps to improve the simulated variability. Besides the variability, systematic FWC errors are found widely existing in current models, which mostly depend on how the model reaches its equilibrium (Wang et al., 2016).

In order to simulate the recent FWC changes, we configured a regional model for the Arctic Ocean. We first investigated the optimization strategies to improve the model performance in simulating both the Atlantic Water and the FWC in the Canada Basin. As a freshwater input, sea surface salinity restoring significantly relieves the salinity drift in the models and improves the hydrography in the Amerasian Basin (Wang et al., 2018b). Besides, the background vertical diffusivity controls the stratification of the ocean column below the mixed layer which is generally shallow in the Arctic Ocean, and modulates the vertical oceanic structure (Zhang and Steele, 2007). The diffusivity caused by eddy activities is another impact factor demonstrated from a series of theoretical and model studies (e.g., Spall, 2013; Manucharyan and Spall, 2016; Yang, 2006). The lateral diffusivity that mimics the eddy transport due to insufficient eddy resolving, however, is normally set to zero in the coarse Arctic models. In this study, a latitude and depth varied diffusivity is applied to represent this effect. Motivated by the aforementioned studies, we implemented these approaches in our model and studied their impacts on the hydrographic simulation.

2. Model description and experiments

2.1. Model

The model is configured as a pan-Arctic, regional sea ice-ocean model based on the Massachusetts Institute of Technology general circulation model (MITgcm; Marshall et al., 1997). The oceanic and sea ice dynamic equations are discretized on the spherical grid, while the North Pole is shifted to the geographical location (135°E, 45°N). Given the locally varied spacing (Fig. 1), it guarantees a high resolution of ~10 km in the

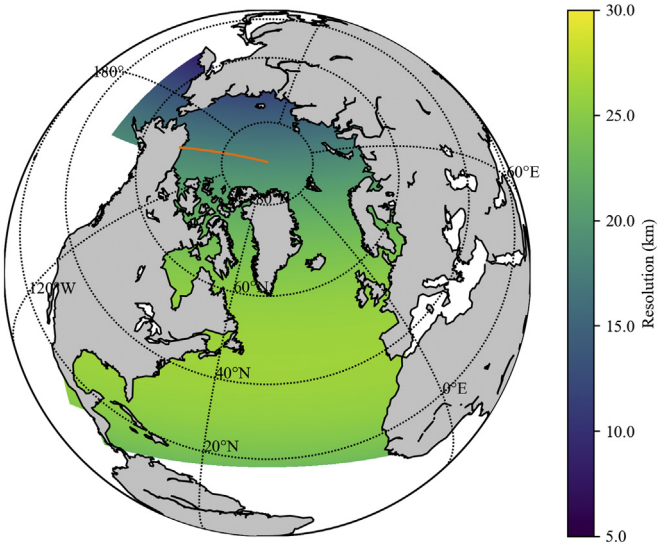

Fig. 1. The model domain and resolution (The orange line defines the section along 150°W ranging from 70°N to 90°N).

Arctic regions while a relatively lower resolution in the lower-mid latitudes to speed up the integration. Although the model is not eddy resolving considering the small baroclinic Rossby radius of deformation which usually is of order 10 km in the Arctic Ocean, most of the Arctic straits and the channels of the Canadian Archipelago are well resolved to achieve a better flux simulation. The southernmost Atlantic boundary is located at 7°N. Compared to other configurations such as in Nguyen et al. (2011) with a southern boundary at ~55°N, our model dramatically reduces the contamination of the boundary condition on the Atlantic Water simulation in the Arctic Ocean. In the Pacific sector, the boundary is cutting across the Aleutian Islands as in most of the regional Arctic models.

The vertical resolution is around 10 m in the first 12 levels then varying slowly to 450 m thick to the depth. Bathymetry is derived from the General Bathymetric Chart of the Oceans (GEBCO) gridded data (https://www.gebco.net). The GEBCO data are remapped onto the model mesh using the Climate Data Operators (CDO) and then smoothed to remove extremely large gradients to stabilize the integration.

The model solves the discretized equations with a time step of 900 s for both ocean and sea ice components. It uses an oceanic state equation of Jackett and McDougall (1995). The vertical eddy viscosity of momentum terms is set to 5.66×10^{-4} m^2 s^{-1}. A vector invariant formulation is used to solve the momentum equations with viscous dissipation computed by the biharmonic Smagorinsky scheme (Smagorinsky, 1963). Background vertical and horizontal diffusivity of tracers is set to 1.0×10^{-5} m^2 s^{-1} and 12.96 m^2 s^{-1}, respectively. For the tracers, a high-order monotonicity-preserving advection scheme is employed (Daru and Tenaud, 2004). The diapycnal mixing is parameterized with the KPP scheme (Large et al., 1994). We used free slip boundary conditions in lateral and no-slip conditions at the bottom.

The sea ice model is configured to use the viscous plastics rheology (Hibler, 1979). The high non-linearity in sea ice

momentum equations are solved by the line successive relaxation (LSR) solver (Zhang and Hibler, 1997). The sea ice strength is parameterized by sea ice concentration and sea ice thickness according to Hibler (1979), and the strength parameter P^* is set to 2.264×10^4 N m^{-2}. In lateral, no-slip conditions are used for sea ice. Surface flux exchanges between atmosphere and ocean/sea ice are calculated with the bulk formula according to Large and Pond (1981). The sea ice thermodynamics have one layer with zero heat capacity (Semtner, 1976; Parkinson and Washington, 1979). Sea ice thickness is divided into seven categories to mimic sea ice growth in the ice thickness distribution (ITD) model (Hibler, 1984). Following Zhang et al. (1998), snow thickness is a prognostic variable. Precipitation converts to snow when the air temperatures are below the freezing point. At the surface grid, a heat balance equation is solved to determine if additional heat can be conducted further down to the bottom. The lead closing parameter during the freezing season is set to 0.6.

Initial ocean hydrography is taken from the Ocean Reanalysis System 5 (ORAS5; Zuo et al., 2019) from the European Centre for Medium-Range Weather Forecasts (ECMWF). For sea ice model, the sea ice concentration, sea ice thickness, salinity of sea ice, and snow thickness are initialized by the Pan-Arctic Ice-Ocean Modeling and Assimilation System datasets (Zhang and Rothrock, 2003). Lateral boundary conditions are constructed by monthly reanalysis data with the product ID GLOBAL_REANALYSIS_PHY_001_030 from the Copernicus Marine Environment Monitoring Service (CMEMS; https://marine.copernicus.eu/).

The model is forced by 3-Hourly atmospheric states from the Japanese 55-year Reanalysis (JRA-55; Kobayashi et al., 2015), which are 10-m surface winds, 2-m temperature, total precipitation, humidity, downward shortwave radiation and downward longwave radiation. The horizontal resolution of these fields is around 0.5625°. The monthly climatological river runoff data are from the Arctic Runoff Database (ARDB), which were also used in Nguyen et al. (2011).

2.2. Experiment design

To get realistic FWC simulation in the recent decade, we considered the effects of horizontal diffusivity, vertical diffusivity, and sea surface salinity restoring in the study. Global ocean models commonly suffer salinity drift due to various reasons, for example, unrealistic freshwater input caused by inaccurate precipitation or river runoff and the numerical walking-around like virtual salinity flux technique. Therefore, we designed four experiments as in Table 1.

The CTRL experiment has a background horizontal Laplacian diffusivity of 12.96 m^2 s^{-1} for temperature and salinity over the entire domain. Background vertical Laplacian diffusivity of tracers are set to 1.0×10^{-5} m^2 s^{-1} globally. No sea surface salinity restoring is applied.

The SSS experiment takes the same values of the horizontal and vertical diffusivity as CTRL, and further applies the sea surface salinity restoring with a timescale of 30.25 d. The monthly climatology of sea surface salinity from the Polar science center Hydrographic Climatology (PHC; Steele et al., 2001) at the University of Washington is used.

Table 1
The list of experiments.

Experiment	Background horizontal Laplacian diffusivity of tracers (m^2 s^{-1})	Background vertical Laplacian diffusivity of tracers (m^2 s^{-1})	Timescale of sea surface salinity restoring (d)
CTRL	12.96	1.0×10^{-5}	–
SSS	12.96	1.0×10^{-5}	30.25
Kh_SSS	Grid dependent from 1500 to 12.96	1.0×10^{-5}	30.25
Kh_Kz_SSS	Grid dependent from 1500 to 12.96	Grid dependent from 1.0×10^{-5} to 5.0×10^{-7}	30.25

The difference of the set-up between the Kh_SSS experiment and the SSS experiment is that Kh_SSS has a latitude dependent background horizontal Laplacian diffusivity that serves as the neutral diffusivity varying from 1500 m^2 s^{-1} in the Atlantic Ocean to 12.96 m^2 s^{-1} in the Arctic Ocean. The diffusivity is then scaled by the squared buoyancy frequency in each depth as that implemented in FESOM (Wang et al., 2014).

The Kh_Kz_SSS experiment further changes the background vertical diffusivity with also a grid dependent value varying from 1.0×10^{-5} to 5.0×10^{-7} m^2 s^{-1}. It is set high in the Atlantic Ocean and low in the Arctic Ocean as inferred from Fig. 1. The latitude dependent structure of diffusivity is motivated by the theoretical study (Müller et al., 1986) and the numerical study (Jochum, 2009) where a latitudinally varied diffusivity was derived based on observational evidences. The sea surface salinity restoring with a timescale of 30.25 d was also used.

All the experiments are driven by the same atmospheric forcing, prescribed with the same boundary conditions, and initialized by the same hydrography as described in Section 2. The integration period is all starting from January 1993 to December 2018. The output from 2007 to 2018 after 14 years from the model beginning was used for the analysis.

3. Results

3.1. Sea ice extent

Fig. 2a shows the sea ice extent simulation of all the experiments. The observed sea ice extent was calculated from the sea ice concentration product with ID OSI-450 (Lavergne et al., 2019) provided in the Ocean and Sea Ice Satellite Application Facility (OSI SAF). All the simulated results agree well with the observation. Specifically, the low sea ice extent records like in 2012 and in 2007 are all reproduced by the model. The annual variability is also consistent with the observation. The model has more sea ice in the early

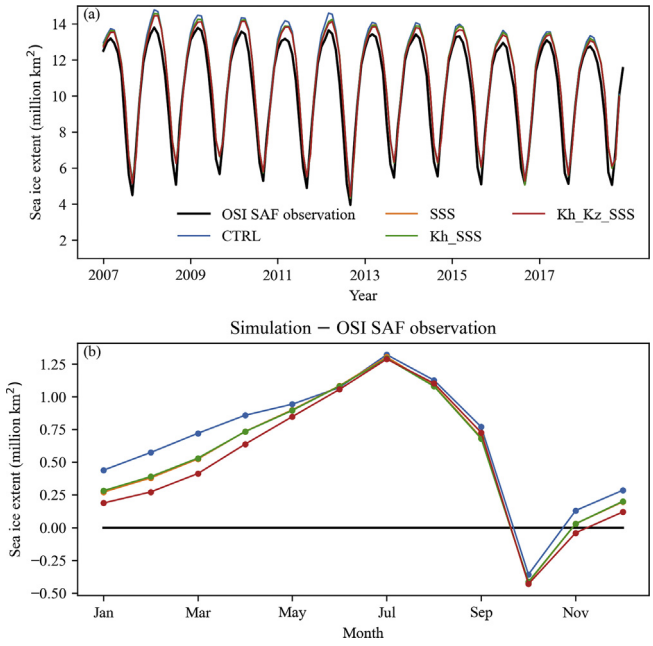

Fig. 2. Monthly mean sea ice extent from 2007 to 2018 (a), and (b) seasonal cycle of the simulation differences against the OSI SAF observations.

summertime. In general, the model shows the ability to represent the critical aspects of observed recent Arctic sea ice changes.

The misfits against the observation in Fig. 2b demonstrate that the most pronounced sea ice extent error occurs in July. The model tends to produce too much sea ice in the freezing season starting from December. The errors decrease after July until it changes its sign to negative in October. Such delayed sea ice melting and growing processes may suggest that the thermodynamic process onset is not well represented in the current sea ice model.

The sea surface salinity restoring helps to mitigate the simulated sea ice extent error as shown in Fig. 2b. The experiments SSS, Kh_SSS, and Kh_Kz_SSS all have smaller errors in all the months except in October. The improvements are more remarkable in the wintertime from November to May in the following year. It indicates that parts of sea ice extent errors are caused by unrealistic sea surface salinity which, however, substantially involves in the calculation of the freezing point.

A weak vertical background diffusivity in the Arctic Ocean improves the sea ice extent simulation. A further reduction of error was observed in the experiment Kh_Kz_SSS compared to that in the experiments SSS and Kh_SSS. As the effects of the sea surface salinity restoring, it also mostly happens in the wintertime. Little effects were observed in the summertime. It indicates that the physical process attributed to the model bias does not take place at the ice bottom but at the surface, for example, by tuning the ice and snow albedos in the melting season. It is worth to be noted that the current model does not contain any melting pond process which is documented to be a crucial precondition to the sea ice melting. Overall, the results suggest that Kh_Kz_SSS provides a good basis for the simulation of upper oceanic hydrography.

3.2. Summer Pacific halocline water

Pacific Summer Water originating from the Pacific Ocean can be divided into two sources: Alaskan Coastal Water (ACW) and summer Bering Sea Water (sBSW) based on their salinity differences (Steele et al., 2004). ACW gains its property along the Alaska coast with salinity between 31 and 32. sBSW overlying Pacific Winter Water (PWW) has a salinity range from 32 to 33. The layers between $S = 31$ and $S = 33$ is the so-called 'summer Pacific halocline water' (Steele et al., 2004). The isohalines of $S = 31$ and $S = 33$ therefore serve as proper proxies to diagnose model performances in the upper ocean (Wang et al., 2018b; Zhang et al., 2016).

In all experiments, the simulated $S = 31$ isohalines change slightly over 2007–2015 (Fig. 3). Then a rapid deepening is observed since 2016, which may result from the lagged ocean response to the episodic extrema of surface stress energy input (Zhong et al., 2019). The seasonal variability is not prominent. The observed isohaline of $S = 31$ lies at the depth of 61.7 m over 2007–2013. Both SSS and Kh_SSS overestimate the depth, although they agree well with observations from 2008 to 2010. CTRL and Kh_Kz_SSS generally have a shallower depth than observations.

For the isohaline $S = 33$, all the simulations show minor seasonal variability (Fig. 3). Kh_Kz_SSS simulates the isohaline $S = 33$ well fit the observations apart from that in 2007. The other experiments, however, are all biased deep. We found a maximum model bias of more than 40 m in these experiments. Their interannual variabilities show some similarities to the observations but too strong.

3.3. Freshwater content

The FWC is defined as $\int_z^0 (S_{\mathrm{ref}} - S)/S_{\mathrm{ref}} \mathrm{d}z'$, where $S_{\mathrm{ref}} = 34.8$ is the reference salinity, and z is the depth where salinity reaches S_{ref}. Recently, debates exist on the physical meaning of FWC which, as defined, using an arbitrarily selected reference salinity that may be totally useless as a benchmark for the assessment of ocean states (Schauer and Losch, 2019). We still used this metric considering the fact that the observations are still provided in FWC.

As described in Section 1, after the rapid accumulation from 2007 to 2008, the observed FWC shows a plateau from 2008 to 2012 although with a slightly increase (black line in Fig. 4a). After the strong freshwater release in 2012/2013, FWC rebounds to its previous level and exhibits a new plateau in 2016–2018, which is approximately 1.5 m larger than that over the previous plateau.

The experiments SSS and Kh_SSS are biased high (~2 m) compared to the observation. They also reproduce a high FWC

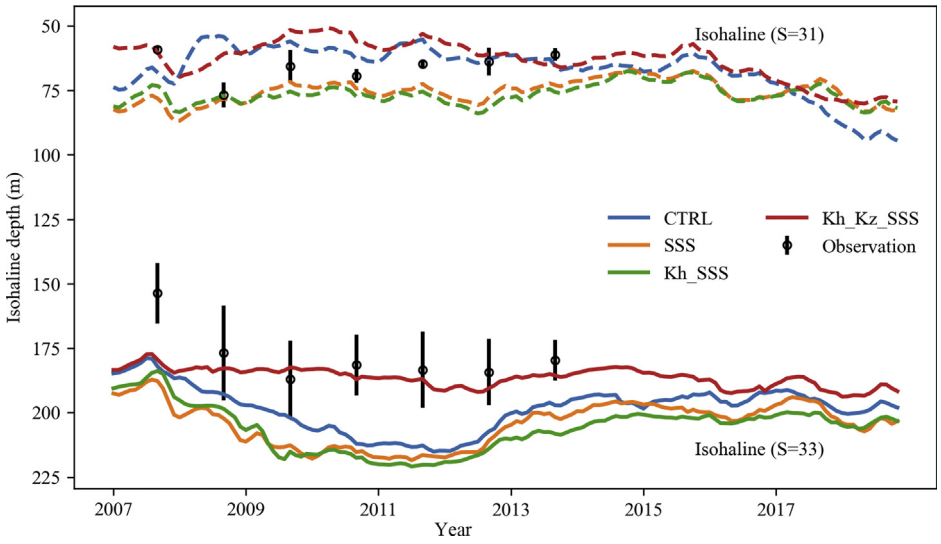

Fig. 3. Depth of isohalines ($S = 31$ and $S = 33$) averaged in the central Beaufort Gyre region boxed by 74°−79°N, 135°−150°W. (Details of the observations (black) are described in Timmermans et al. 2014). Observation errors are shown by error-bars).

during 2008−2012, but the even higher FWC over 2016−2018 in the observation is not well simulated. The CTRL experiment shows higher FWC over the second plateau period but does not form a plateau. Model bias about 1.5 m is also observed in CTRL (Fig. 4b).

The experiment Kh_Kz_SSS (red line in Fig. 4a) has the least deviation to the observation. It reproduces low FWC bias over the first plateau period and the rapid increasing in 2015/2016, thereafter, higher FWC is found over the second plateau years as observed. The fast freshwater release in 2012/2013 and the accumulation event in 2014 however are not well simulated. The multi-year mean FWC shown in Fig. 4b also demonstrates that Kh_Kz_SSS is biased low with an error of ~0.7 m.

FWC has strong seasonal variability (Fig. 4b), which is also described in Hu et al. (2019). The FWC increases when sea ice starts melting from May, and reaches its annual maximum in October, then falls due to freezing. All the model simulations exhibit the same interannual variability although with different amplitudes, for example, the decline from 2014 to 2015. This suggests that the same physical process in these simulations is responsible for the model errors.

4. Discussion

4.1. The impact on the simulation of sea ice edge and volume transport

Fig. 5 shows that the model well agrees with the sea ice observation in the Pacific sector and the Labrador Sea. Large discrepancies are found in the Greenland Sea where complicated processes such as deep convection and eddy activity often occur, which are both large error sources for current models. As discussed in Section 3.1, employing sea surface salinity restoring and a weak background vertical diffusivity we found improved sea ice extent simulation. However, the improvement is rather minor.

Sea ice in the Greenland Sea and the Barents Sea suggests that sea surface salinity restoring helps mostly over the recirculation area south of Svalbard Island and northwest of the Barents Sea. It also has positive effects in the southern Bering Sea. Tuning the background vertical diffusivity does not make too much difference in the North Atlantic sector and the Pacific sector, but it can be found that experiment with both sea surface salinity restoring and vertical diffusivity tuning simulates sea ice edge closer to the observation. Therefore, in addition to the effects of the thermodynamic processes on the sea ice component, the discrepancy to represent realistic sea surface salinity in the model is another large error source for the sea ice simulation. The background vertical and horizontal diffusivity, however, has limited impacts.

Moreover, sea surface salinity restoring has dramatically improved the hydrographic simulation in the North Atlantic. Due to the model bias on sea ice simulation, freshwater output from the Arctic Ocean desalinates the North Atlantic after long-term integration in our model, although it could be a different story in other models due to different model drift direction. The desalination enhances the stratification of the ocean column and further prevents the ocean heat release in the Atlantic Ocean. Therefore, excessive warming of the Atlantic Water is found in the Arctic Ocean in the CTRL experiment (Figure not shown).

We also investigated the volume flux across the main gateways such as the Fram Strait, Barents Sea Opening, Bering Strait, and Davis Strait in the Arctic Ocean. Due to the open boundary condition prescribed over south of the Bering Sea, the volume flux for different experiments across the Bering Strait is identical (~1.2 Sv). The restoring of sea surface salinity significantly improves the volume flux from 0.7

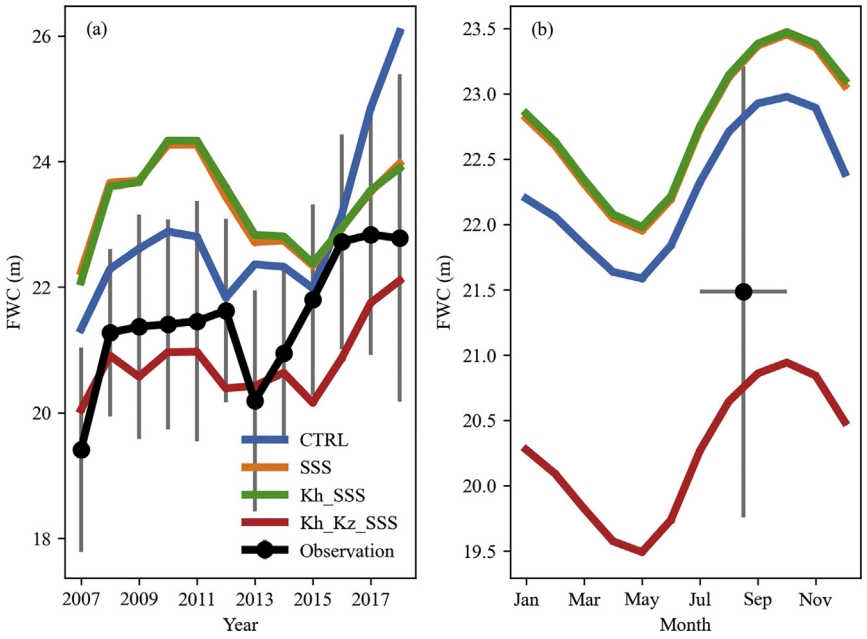

Fig. 4. The simulated and observed FWC in July−October in the Beaufort Sea from 2007 to 2018 (a), and (b) annual cycle of FWC variations of the period over the same region (The black dot gives the mean observed FWC in July−October. The vertical grey bar shows the observation error, while the horizontal error bar indicates the observation as the mean value of that from July through October. The readers are referred to Proshutinsky et al. (2009) for details about the observations).

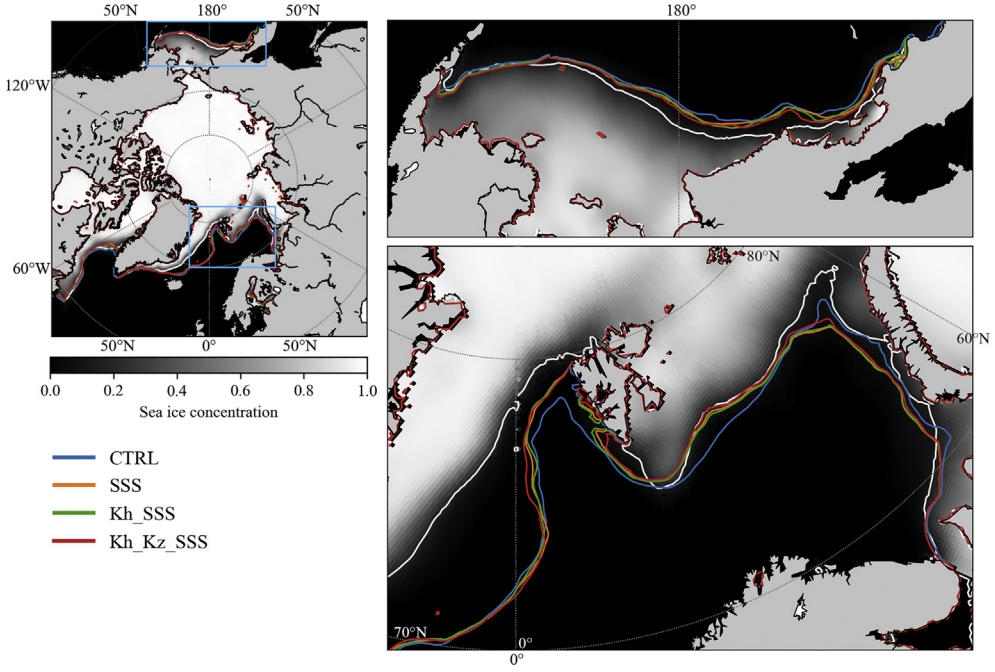

Fig. 5. Sea ice concentration in March averaged over 2007−2018 (The cyan boxes in the left panel are zoomed respectively in the right column. Sea ice edge defined as 0.15 sea ice concentration contour is shown for each experiment. OSI SAF sea ice edge is shown in white contour).

Sv to 1.5 Sv across the Davis Strait, which corresponds well to the observation range (1.6 Sv−2.1 Sv). Minor differences of the volume flux are found between the experiments with and without enhanced background horizontal diffusivity. A weaker vertical diffusivity in the Arctic Ocean modulates 10% at most of the volume flux over the Barents Sea Opening and Fram Strait. The variability of the volume flux over different gateways changes even smaller.

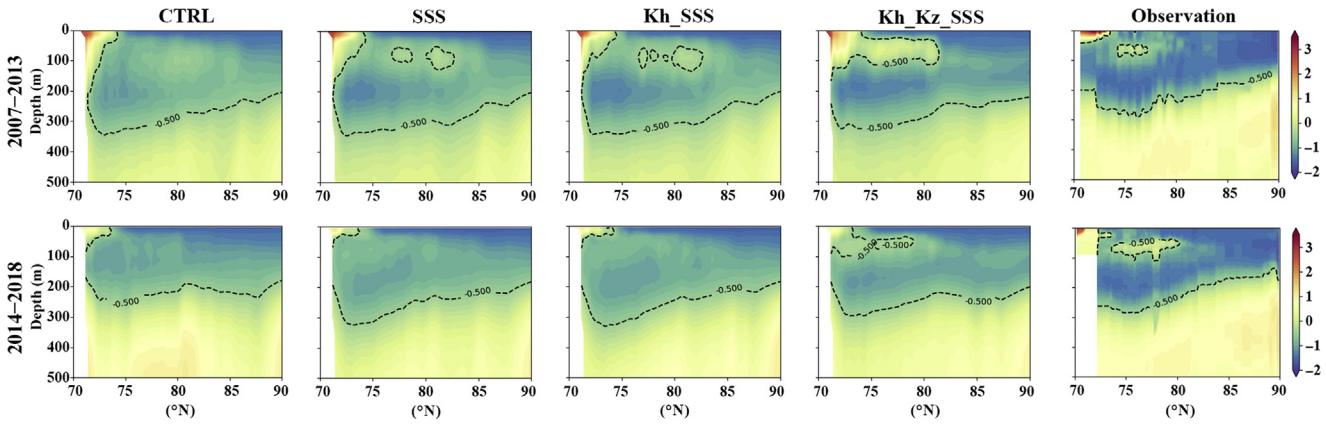

Fig. 6. Hovmöller diagram of mean temperature at the transect along the 150°W averaged over August–October for periods 2007–2013 and 2014–2018 (The observations over the same periods are obtained from the World Ocean Database 2018 (https://www.nodc.noaa.gov/OC5/WOD/pr_wod.html). The section of 150°W is defined ranging from 70°N to 90°N with a width of 50 km (see Fig. 1). Contour lines of −0.5 °C are shown both in the simulations and observations).

4.2. A weak background vertical diffusivity preserves the vertical structure of PSW

Due to the presence of sea ice, the energy input into the ocean is dissipated mostly at the ocean surface. Therefore, the diffusivity is commonly reported as small in the central Arctic Ocean. The vertical diffusivity estimated by mooring observations in the Beaufort Gyre ranges from 3×10^{-7} to 3×10^{-5} m^2 s^{-1} between 150 m and 400 m but can reach 10^{-4} m^2 s^{-1} when a strong process occurs (Lique et al., 2014). For the upper ocean, results from Surface Heat Budget of the Arctic Ocean (SHEBA) field program reveal that the diffusivity in the Canada Basin is rather at the molecular level in wintertime (Shaw and Stanton, 2014). In the model, with a weak background vertical diffusivity, it is possible for us to maintain a realistic vertical structure of PSW as shown in Figs. 6 and 7.

A temperature maximum of the upper 150 m in the Canada Basin is the typical character of PSW (Steele et al., 2004). In the observations, we found prominent PSW temperature maxima both over 2007–2013 and 2014–2018 (Fig. 6). It is captured by all the experiments with sea surface salinity restoring over 2007–2013. However, only the experiment Kh_Kz_SSS with weak vertical diffusivity reproduces the PSW temperature maxima over 2014–2018 (Fig. 6). The ventilation of warm halocline near the continental shelf during summertime in Kh_Kz_SSS also agrees well with the observations and current understanding (Timmermans et al., 2017). The vertical distribution of temperature in CTRL experiment is rather uniform. The upper ocean is sufficiently mixed in this experiment where much warmer Pacific Winter Water is observed than that in other experiments.

Moreover, the isohalines as shown in Fig. 7 in the experiment Kh_Kz_SSS consistently correspond to the observations. The distance between isohalines $S = 31$ and $S = 33$ is gradually narrowing with latitude increasing, which coincides with the observed oceanographic section towards the Lomonosov Ridge. The isohaline of $S = 33$ in other experiments is horizontally flatter. This explains the good agreement of Kh_KZ_SSS in simulating the isohaline $S = 33$ depth in Fig. 3.

Compared to the experiment SSS, Kh_SSS does not change the results a lot. It suggests that the background horizontal

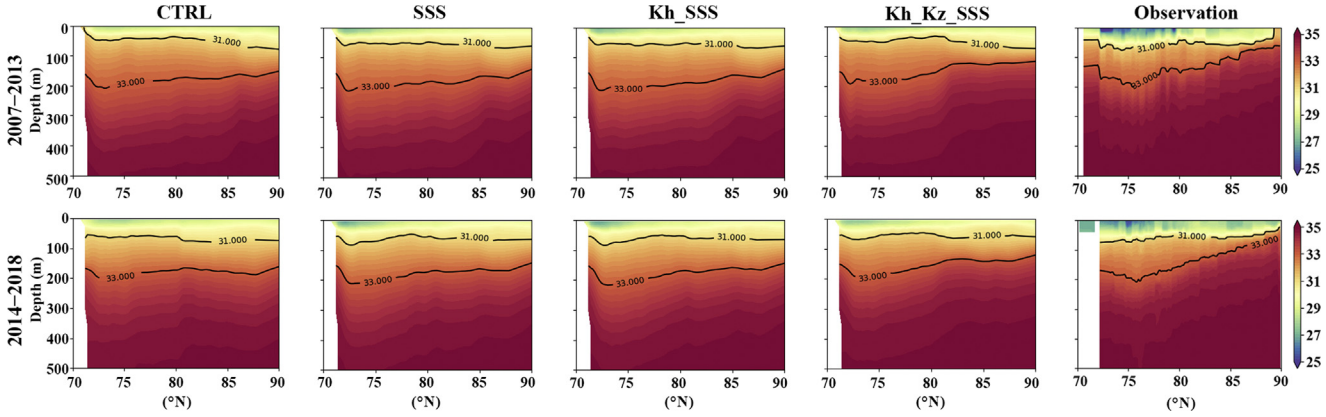

Fig. 7. Hovmöller diagram of mean salinity at the transect along the 150°W averaged over August–October for periods 2007–2013 and 2014–2018. The observations over the same periods are obtained from the World Ocean Database 2018. The section of 150°W is defined ranging from 70°N to 90°N with a width of 50 km (see Fig. 1). Contour lines of 31 psu and 33 psu are highlighted in each plot.

diffusivity in our model is not of the first order on the hydrographic simulation in the Canada Basin. Using a larger horizontal diffusivity majorly improve the temperature simulation in the North Atlantic Ocean (Figure not shown).

5. Conclusion

A new pan-Arctic sea ice-ocean model was configured based on MITgcm. To obtain realistic simulations, we studied the impact of sea surface salinity restoring, horizontal and vertical background diffusivity on sea ice, and the upper ocean simulation in the Canada Basin.

With sensitivity experiments, we found that applying the sea surface salinity restoring gives rise to better sea ice edge simulation and more realistic sea surface temperature in the North Atlantic, although the latter is not explicitly discussed. The tuning experiment further using latitude varied horizontal background diffusivity changes the simulated results very small. When applying a weak background vertical diffusivity of 5.0×10^{-7} m^2 s^{-1}, the model reproduces slightly better sea ice simulation and maintains the vertical hydrographic structure well fit to the observations in the Canada Basin. We found that the sea ice variability is not remarkably changed by these sensitivity experiments. However, the sea surface salinity restoring has suppressed the ocean variabilities as expected, where minor changes are observed on the variabilities of the volume flux across the gateways in the Arctic Ocean. The volume flux over the Davis Strait is subject to the surface restoring, which is more sensitive than that over other gateways.

Since the sea surface salinity restoring is also a source of freshwater input, modeling the freshwater in the upper ocean is more or less a tug-of-war between the vertical diffusivity and the restoring strength. Note that sea surface salinity restoring in current study is quite strong. The simulation could be further improved by using a weaker restoring, for example, 60 days, as most models in the Coordinated Ocean-ice Reference Experiments, phase II. Future work will focus on the improvement of the sea ice simulation in the Greenland Sea.

Declaration of competing interest

The authors declare no conflicts of interest.

Acknowledgment

This study was supported by the National Natural Science Foundation of China (42176235) and the National Key Research and Development Program of China (2019YFA0607000 and 2019YFC1509100). The simulations were performed on the supercomputer Ollie at the Alfred Wegener Institute (AWI) Helmholtz Centre for Polar and Marine Research supported by the Federal Ministry of Education and Research of Germany in the framework of SSIP (01LN1701A). We thank the Ocean Data View (ODV) provides the personal license for figure plotting.

References

Daru, V., Tenaud, C., 2004. High order one-step monotonicity-preserving schemes for unsteady compressible flow calculations. J. Comput. Phys. 193 (2), 563−594.

Hibler III, W.D., 1979. A dynamic thermodynamic sea ice model. J. Phys. Oceanogr. 9 (4), 815−846.

Hibler III, W.D., 1984. The role of sea ice dynamics in modeling CO_2 increases. Clim. Proc. Clim. Sens. 29, 238−253.

Hu, X., Myers, P.G., Lu, Y., 2019. Pacific Water pathway in the Arctic Ocean and Beaufort Gyre in two simulations with different horizontal resolutions. J. Geophys. Res. Oceans 124 (8), 6414−6432.

Jackett, D.R., Mcdougall, T.J., 1995. Minimal adjustment of hydrographic profiles to achieve static stability. J. Atmos. Ocean. Technol. 12 (2), 381−389.

Jochum, M., 2009. Impact of latitudinal variations in vertical diffusivity on climate simulations. J. Geophys. Res. Oceans 114 (C1). https://doi.org/10.1029/2008JC005030.

Kobayashi, S., Ota, Y., Harada, Y., et al., 2015. The JRA-55 reanalysis: general specifications and basic characteristics. J. Meteorolog. Soc. Jpn. Ser. II 93 (1), 5−48.

Large, W.G., Pond, S., 1981. Open ocean momentum flux measurements in moderate to strong winds. J. Phys. Oceanogr. 11 (3), 324−336.

Large, W.G., McWilliams, J.C., Doney, S.C., 1994. Oceanic vertical mixing: a review and a model with a nonlocal boundary layer parameterization. Rev. Geophys. 32 (4), 363−403.

Lavergne, T., Sørensen, A.M., Kern, S., et al., 2019. Version 2 of the EUMETSAT OSI SAF and ESA CCI sea-ice concentration climate data records. Cryosphere 13 (1), 49−78.

Lique, C., Guthrie, J.D., Steele, M., et al., 2014. Diffusive vertical heat flux in the Canada Basin of the Arctic Ocean inferred from moored instruments. J. Geophys. Res. Oceans 119 (1), 496−508.

Manucharyan, G.E., Spall, M.A., 2016. Wind-driven freshwater buildup and release in the Beaufort Gyre constrained by mesoscale eddies. Geophys. Res. Lett. 43 (1), 273−282.

Marshall, J., Adcroft, A., Hill, C., et al., 1997. A finite-volume, incompressible Navier Stokes model for studies of the ocean on parallel computers. J. Geophys. Res. Oceans 102 (C3), 5753−5766.

Müller, P., Holloway, G., Henyey, F., et al., 1986. Nonlinear interactions among internal gravity waves. Rev. Geophys. 24 (3), 493−536.

Nguyen, A.T., Menemenlis, D., Kwok, R., 2011. Arctic ice-ocean simulation with optimized model parameters: approach and assessment. J. Geophys. Res. Oceans 116 (C4). https://doi.org/10.1029/2010JC006573.

Parkinson, C.L., Washington, W.M., 1979. A large-scale numerical model of sea ice. J. Geophys. Res. Oceans 84 (C1), 311−337.

Proshutinsky, A., Krishfield, R., Timmermans, M.L., et al., 2009. Beaufort Gyre freshwater reservoir: state and variability from observations. J. Geophys. Res. Oceans 114 (C1). https://doi.org/10.1029/2008JC005104.

Rabe, B., Karcher, M., Kauker, F., et al., 2014. Arctic Ocean basin liquid freshwater storage trend 1992−2012. Geophys. Res. Lett. 41 (3), 961−968.

Schauer, U., Losch, M., 2019. "Freshwater" in the ocean is not a useful parameter in climate research. J. Phys. Oceanogr. 49 (9), 2309−2321.

Semtner Jr., A.J., 1976. A model for the thermodynamic growth of sea ice in numerical investigations of climate. J. Phys. Oceanogr. 6 (3), 379−389.

Serreze, M.C., Barry, R.G., 2011. Processes and impacts of Arctic amplification: a research synthesis. Global Planet. Change 77 (1−2), 85−96.

Shaw, W.J., Stanton, T.P., 2014. Vertical diffusivity of the western Arctic Ocean halocline. J. Geophys. Res. Oceans 119 (8), 5017−5038.

Smagorinsky, J., 1963. General circulation experiments with the primitive equations: I. The basic experiment. Mon. Weather Rev. 91 (3), 99−164.

Spall, M.A., 2013. On the circulation of Atlantic water in the Arctic Ocean. J. Phys. Oceanogr. 43 (11), 2352−2371.

Steele, M., Morley, R., Ermold, W., 2001. PHC: a global ocean hydrography with a high quality Arctic Ocean. J. Clim. 14, 2079−2087.

Steele, M., Morison, J., Ermold, W., et al., 2004. Circulation of summer Pacific halocline water in the Arctic Ocean. J. Geophys. Res. Oceans 109 (C2). https://doi.org/10.1029/2003JC002009.

Stroeve, J., Notz, D., 2015. Insights on past and future sea-ice evolution from combining observations and models. Global Planet. Change 135, 119−132.

Tilling, R.L., Ridout, A., Shepherd, A., et al., 2015. Increased Arctic sea ice volume after anomalously low melting in 2013. Nat. Geosci. 8 (8), 643−646.

Timmermans, M.L., Proshutinsky, A., Golubeva, E., et al., 2014. Mechanisms of Pacific Summer Water variability in the Arctic's Central Canada Basin. J. Geophys. Res. Oceans 119 (10), 7523−7548.

Timmermans, M.L., Marshall, J., Proshutinsky, A., et al., 2017. Seasonally derived components of the Canada Basin halocline. Geophys. Res. Lett. 44 (10), 5008−5015.

Wang, Q., Danilov, S., Sidorenko, D., et al., 2014. The Finite Element Sea Ice-Ocean Model (FESOM) v. 1.4: formulation of an ocean general circulation model. Geosci. Model Dev. (GMD) 7 (2), 663−693.

Wang, Q., Ilicak, M., Gerdes, R., et al., 2016. An assessment of the Arctic Ocean in a suite of interannual CORE-II simulations. Part II: liquid freshwater. Ocean Model. 99, 86−109.

Wang, Q., Wekerle, C., Danilov, S., et al., 2018a. Arctic sea ice decline significantly contributed to the unprecedented liquid freshwater accumulation in the Beaufort Gyre of the Arctic Ocean. Geophys. Res. Lett. 45 (10), 4956−4964.

Wang, Q., Wekerle, C., Danilov, S., et al., 2018b. A 4.5 km resolution Arctic Ocean simulation with the global multi-resolution model FESOM1.4. Geosci. Model Dev. (GMD) 11, 1229−1255.

Yang, J., 2006. The seasonal variability of the Arctic Ocean Ekman transport and its role in the mixed layer heat and salt fluxes. J. Clim. 19 (20), 5366−5387.

Zhang, J., Hibler III, W.D., 1997. On an efficient numerical method for modeling sea ice dynamics. J. Geophys. Res. Oceans 102 (C4), 8691−8702.

Zhang, J., Rothrock, D.A., 2003. Modeling global sea ice with a thickness and enthalpy distribution model in generalized curvilinear coordinates. Mon. Weather Rev. 131 (5), 845−861.

Zhang, J., Hibler III, W.D., Steele, M., et al., 1998. Arctic ice-oceanmodeling with and without climate restoring. J. Phys. Oceanogr. 28, 191−217.

Zhang, J., Steele, M., et al., 2007. Effect of Vertical Mixing on the Atlantic Water Layer Circulation in the Arctic Ocean. J. Geophys. Res. 112 (C04S04). https://doi.org/10.1029/2006JC003732.

Zhang, J., Steele, M., Runciman, K., et al., 2016. The Beaufort Gyre intensification and stabilization: a model-observation synthesis. J. Geophys. Res. Oceans 121 (11), 7933−7952.

Zhong, W., Zhang, J., Steele, M., et al., 2019. Episodic extrema of surface stress energy input to the western Arctic Ocean contributed to step changes of freshwater content in the Beaufort Gyre. Geophys. Res. Lett. 46 (21), 12173−12182.

Zuo, H., Balmaseda, M.A., Tietsche, S., et al., 2019. The ECMWF operational ensemble reanalysis−analysis system for ocean and sea ice: a description of the system and assessment. Ocean Sci. 15 (3), 779−808.